University of Groningen

Decreased Effective Macromolecular Crowding in Escherichia coli Adapted to Hyperosmotic Stress

Liu, Boqun; Hasrat, Zarief; Poolman, Bert; Boersma, Arnold J

Document Version
Final author's version (accepted by publisher, after peer review)

Link to publication in University of Groningen/UMCG research database

1   **Decreased Effective Macromolecular Crowding in *Escherichia coli* Adapted to**

2   **Hyperosmotic Stress**

3

4   Boqun Liu,[a,b] Zarief Hasrat,[a] Bert Poolman,[a,c]# Arnold J. Boersma[a,d]#

5   [a] Department of Biochemistry, Groningen Biomolecular Sciences and Biotechnology Institute,

6   University of Groningen, Groningen, The Netherlands

7   [b] Jilin Provincial Key Laboratory of Nutrition and Functional Food, Jilin University,

8   Changchun, People's Republic of China

9   [c] Zernike Institute for Advanced Materials, University of Groningen, Groningen, The

10   Netherlands

11   [d] DWI-Leibniz Institute for Interactive Materials, Aachen, Germany

12

13   Running Head: Macromolecular Crowding under Hyperosmotic Stress

14   **# Address Correspondence to**: Bert Poolman, b.poolman@rug.nl and Arnold J. Boersma,

15   boersma@dwi.rwth-aachen.de

18

19

20

21

22

ABSTRACT *Escherichia coli* adapts to changing environmental osmolality to survive and maintain growth. It has been shown that GFP diffusion in cells adapted to osmotic upshifts is higher than expected from the increase in biopolymer volume fraction. To better understand the physicochemical state of the cytoplasm in adapted cells, we now follow the macromolecular crowding during adaptation with FRET-based sensors. We apply an osmotic upshift and find that, after an initial increase, the apparent crowding decreases over the course of hours, to arrive at a value lower than before the osmotic upshift. Crowding relates to cell volume until cell division ensues, after which a transition in the biochemical organization occurs. Analysis of single cells by microfluidics shows that changes in cell volume, elongation and division are most likely not the cause for the transition in organization. We further show that the decrease in apparent crowding upon adaptation is similar to the apparent crowding in energy-depleted cells. Based on our findings in combination with literature data, we suggest that adapted cells have indeed an altered biochemical organization of the cytoplasm, possibly due to different effective particle-size distributions and concomitant nanoscale heterogeneity. This could potentially be a general response to accommodate higher biopolymer fractions yet retaining crowding homeostasis, and could apply to other species or conditions as well.

IMPORTANCE Bacteria adapt to ever changing environmental conditions such as osmotic stress and energy limitation. It is not well understood how biomolecules reorganize themselves inside *Escherichia coli* under these conditions. An altered biochemical organization would affect macromolecular crowding, which could influence reaction rates and diffusion of macromolecules. In cells adapted to osmotic upshift, protein diffusion is indeed faster than expected on the basis of the biopolymer volume fraction. We now probe the effects of macromolecular crowding in cells adapted to osmotic stress or depleted in metabolic energy with a genetically encoded fluorescence-based probe. We find that the effective macromolecular crowding in adapted and energy-depleted cells is lower than in unstressed cells, indicating major alterations in the biochemical organization of the cytoplasm.

INTRODUCTION

The environment induces changes in the internal organization of a cell, for example during

nutrient depletion or osmotic changes. Nutrient depletion halts diffusion of 100 nm-sized

particles,(1) while osmotic stress decreases the diffusion of 10 nm-sized proteins.(2, 3) Cells

adapt to environmental stresses to resume growth, but their internal structure may be

changed. For instance, the lateral diffusion coefficient of GFP in cells adapted to osmotic

stress is higher than expected from the biopolymer volume fraction.(4) The cytoplasmic

structure, or biochemical organization, can influence GFP diffusion in various ways, for

example by changing the microscopic viscosity, association of proteins with (non)specific

binding partners, the presence of barriers such as membrane invaginations, or sieving

effects by for example the nucleoid or transertions.(2, 4-6) Thus, the change in diffusion

indicates that the biochemical organization has undergone a change, but the nature of this

transition is not well understood.

One important aspect of cell physiology is macromolecular crowding,(7-10) which influences

lateral diffusion but also induces excluded volume effects. The steric repulsion between a

high concentration of biomacromolecules ("crowders") reduces the configurational entropy of

these crowders. A biochemical reaction ("tracer") that takes place in this environment

reduces its volume to maximize the configurational entropy for the crowders. This effect can

especially drive large complexes together where crowders are excluded from the volumes in

between the tracers (overlap volumes). In this manner, the excluded volume provides an

additional force to sort biomolecules to provide biochemical organization by favoring

(supra)molecular complexes and membraneless compartments. Excluded volume effects are

increased when for example: (i) the crowders are actually mobile and can increase their

translational degrees of freedom; and (ii) when they are smaller in size than the tracer.(11)

Thus, immobile crowders and/or crowders that are larger than the tracer is display less of the

crowding effect in the classical sense but can induce confinement, where the shape of the

confinement enforces a shape onto the tracer, instead of the minimum volume obtained in

78 classical crowding. Macromolecular crowding, or excluded volume effects, therefore does not

79 necessarily correlate with the biopolymer volume fraction.

80 Macromolecular crowding is one of the main parameters that changes when the volume of a

81 cell changes, which can occur when the medium osmolality changes. Upon osmotic upshift,

82 the cells immediately shrink and many cells counteract this by taking up potassium ions,

83 which is best documented for *E. coli*.(12-14) Subsequently, *E. coli* synthesizes or takes up

84 available compatible solutes, and adjusts the proteome to adapt to the osmotic upshift.

85 Researchers showed that in *E. coli* over 300 genes are up- or downregulated by osmotic

86 upshift.(15-17) *E. coli* further increases its RNA/protein ratio due to an increase in ribosome

87 content when adapted to high osmotic strength,(18) possibly to compensate for the

88 decreased rate of translation.

89 We apply here a set of FRET-based sensors that enable quantification of macromolecular

90 crowding during adaptation to osmotic stress. The sensors have shown excellent

91 performance in quantification of crowding during osmotic stress in mammalian cells,(19-21)

92 and allow detailed analysis of crowding in the bacterium *Escherichia coli*.(19, 22) The

93 sensors vary in size, with crGE being the largest probe with a linker region that contains two

94 α-helices and three random coils in between the fluorescent proteins that form a FRET pair

95 (mCerulean3 as donor and mCitrine as acceptor). The crE6G2 sensor contains a linker with

96 two α-helices and a small random coil, while the crG18 probe contains a single long random

97 coil.

98 Using these probes, we show here that macromolecular crowding increases upon osmotic

99 upshift and returns within 2-5 hours to a level lower than the crowding prior the osmotic shift.

100 We explain the lower effective excluded volume with the hypothesis that the biochemical

101 organization of the cytoplasm is significantly altered, with components that exert less

102 excluded volume effects for molecules in the size-range of our molecular probes.

103

104 **MATERIALS AND METHODS**

105 **Cell growth and confocal imaging.** Cell preparation, growth, and imaging were performed

106 as described in (19, 22). Briefly, the pRSET A vector containing the synthetic gene encoding

107 either crGE, crE6G2 or crG18 was transformed into *E. coli* BL21(DE3). The cells were

108 incubated at 30 °C, shaking at 200 rpm, in 10 mL MOPS medium pH 7.2 with 20mM glucose

109 and grown overnight. The next day, the cells were diluted into 50 mL of fresh medium to

110 OD_{600}=0.05. When the OD_{600} reached 0.1 – 0.2, the cells were imaged. Subsequently, the

111 concentration of NaCl was raised to 300 mM by addition of pre-warmed 3M NaCl in MOPS

112 medium, and the cells were imaged to follow their recovery. The OD_{600} was monitored in

113 time, and the cell culture was diluted with pre-warmed medium (MOPS medium + 300 mM

114 NaCl) to reduce the OD_{600} every time from 0.3 to 0.1. For imaging, a 0.5 mL sample of cells

115 expressing one of the probes was combined with 0.5 mL of cells that contained monovalent

116 streptavidin in pRSET A (blank). A parallel culture was maintained under the same conditions

117 to provide the blank cells. The combined cells were 10× concentrated by centrifugation and

118 resuspended. Subsequently, 10 µL of the cells was transferred to a glass slide modified with

119 (3-aminopropyl) triethoxysilane and imaged on a laser-scanning microscope (Zeiss LSM

120 710). The probes were excited using a 405-mm LED, and the emission was split into a 450–

121 505 (mCerulean3) and 505–797 nm (FRET) channel. The fluorescence intensities for each

122 cell were determined in ImageJ, and background originating from the blank cells was

123 subtracted.

124 **Imaging in a microfluidics chamber.** The microfluidic chamber (CellASIC ONIX Microfluidic

125 Plates) was pre-warmed overnight at 30 °C on the laser-scanning confocal microscope. The

126 *E. coli* BL21(DE3) with desired crowding probe and the control strain containing monovalent

127 streptavidin were grown overnight to an OD_{600} of 0.1-0.3, which is still in the exponential

128 growth phase, and they were then diluted to OD_{600}=0.01 in MOPS-glucose minimal medium

129 and subsequently loaded in the microfluidic chamber. After loading, the cells were incubated

130 with 0.1× MOPS-glucose medium (MOPS-glucose medium diluted 10× with 0.16 M NaCl) at

131   30 °C for 2h. After 2h, the medium in the microfluidics was replaced by 0.1×MOPS-glucose

132   medium that contained an additional 0.3 M NaCl on top of the 0.16 M. Alternatively, we used

133   600 mM and 1 M sorbitol instead of the 0.3M NaCl for osmotic upshift in the microfluidic

134   chamber. The images were collected and analyzed as described above.

135   **Cell volume determination.** The volume of the cytoplasm was determined by

136   PhotoActivated Localization Microscopy (PALM). The gene encoding LacY was fused to

137   YPet which can switch "on" or "off" during imaging in PALM.(23) The gene encoding LacY-

138   YPet was cloned into the pACYC vector and transformed into *E. coli* BL21(DE3). The cells

139   (inoculated from a single colony) were grown at 30 °C, shaking at 200 rpm, in 10 mL MOPS

140   medium with 20 mM glucose, overnight. The next day, at $OD_{600} = 0.2$, the cells were induced

141   with 0.1% L-rhamnose. One hour after induction, the cells were imaged by PALM microscopy

142   before and after addition of 300 mM NaCl.

143   Coverslips were cleaned with 5 M KOH in a sonication bath for 30 minutes, and washed with

144   demineralized water and acetone (Aldrich). Next, the coverslips were plasma-cleaned for 10

145   min, and subsequently coated with 2% (v/v) (3-Aminopropyl) trioxysilane (Aldrich) in acetone

146   for 30 minutes. The coverslips were washed with demineralized water and left drying.

147   For PALM, a home-built inverted microscope based on an Olympus IX-81 with a high

148   numerical aperture objective (100 X, NA= 1.49, oil immersion, Olympus, UApo) was used.

149   Solid-state lasers were from Coherent (Santa Clara, USA): 514 nm (Sapphire 514, 100 mW).

150   Imaging was performed in semi-TIRF mode with the angle of light exiting the objective

151   adjusted to create a light sheet restricted to the bottom few micrometers of the specimen.

152   The fluorescence was recorded using an electron multiplying charge-coupled device (EM-

153   CCD camera) from Hamamatsu, Japan, model C9100-13. For data acquisition and analysis,

154   LacY-YPet was continuously illuminated at 517 nm and 3000 frames were recorded with 30

155   ms for each frame. The data was analyzed with a home-written ImageJ script, in which the

156   reconstructed images of each fluorescent molecule are represented as a single spot at its

157   determined coordinates, with a brightness that corresponds to the localization accuracy.(23)

158   **Preparation of cell lysate.** The *E. coli* BL21(DE3) cells were incubated in 10 mL MOPS with

159   20 mM glucose at 30 °C and shaking at 200 rpm overnight, and then diluted to 1 L of fresh

160   medium to OD_{600}=0.02. When the OD_{600} reached 0.2, half of the culture was lysed

161   immediately, while the other half was lysed after incubation for 5 h with 300 mM NaCl. To

162   lyse the cells, the cultures were harvested by centrifugation (3000 xg, 30 minutes). The pellet

163   was resuspended in 10 mM NaPi, 100 mM NaCl, pH 7.4, containing proteinase inhibitor

164   (cOmplete™, Mini, EDTA-free). Cells were lysed by sonication for 2 minutes, with alternating

165   5 seconds sonication and 5 seconds cooling, and then centrifuged (20,000xg, 10 min). The

166   supernatant was immediately used for the fluorescence measurements.

167   **Fluorometry**. Fluorescence emission spectra were measured with a Fluorolog-3 (Jobin

168   Yvon) spectrofluorometer. A 1.0 mL solution (10 mM NaPi, 100 mM NaCl, 2 mg/ml BSA, pH

169   7.4) was added to a quartz cuvette and its fluorescence emission spectrum was recorded

170   after excitation at 420 nm (A). Subsequently, purified sensor was added, mixed by pipette,

171   and the fluorescence was recorded (B). The desired amount of small molecule or cell lysate

172   was added, mixed by pipette, and the fluorescence was recorded again (C). The background

173   spectrum A, prior to the addition of the probe, was subtracted from B or C.

174   **OD_{600} measurements during FCCP treatment**. A 96-well plate (Greiner) containing four

175   batches of each of the different culture/condition combinations (200 µL/well), with the

176   remaining wells filled with either filter-sterilized MOPS-glucose minimal medium or MQ water.

177   The plate was covered with gas permeable film and mounted on a plate reader (BioTek

178   PowerWave 340). While shaking the plate at 30 °C, the absorbance at 600 nm was read

179   every minute for 3.5 hours using Gen 5 software. After the plate reader measurement, the

180   OD_{600} values were referenced to the average of the absorbance values for MQ water, for

181   each specific time point.

182

183

184 **RESULTS**

185 **Macromolecular crowding decreases after an osmotic upshift**. To determine the

186 crowding during adaptation to an osmotic upshift, we added 300 mM NaCl to exponentially

187 growing *E. coli* BL21(DE3) and allowed the cells to adapt to the increased medium

188 osmolarity. To monitor the macromolecular crowding, we expressed the crGE probe under

189 leaky expression of the T7 promoter, which prevents maturation artifacts as we described

190 previously.(24) To compare our results with literature data, we performed the experiments in

191 MOPS-glucose medium.(2, 4, 18) We find that under these conditions, the osmotic upshift

192 initially decreases the OD_{600} of the cell culture, which slowly recovers to pre-upshift levels

193 over about an hour. After this, the cultures maintain a steady growth rate throughout the

194 experiments (Fig. 1A).

195 We took samples from the main culture for analysis by confocal fluorescence microscopy and

196 excited the crGE probe at 405 nm, and determined the emission between 450-505 nm for

197 mCerulean3 and 505-795 nm for the FRET channel, as described previously.(19) Before the

198 upshift, the FRET/mCerulean3 is 1.06 ± 0.009 (s.e.m.; n = 98; s.d.=0.07), which immediately

199 increases to 1.12 ± 0.01 (s.e.m.; n = 98) upon addition of 300 mM NaCl (Fig. 1B). These

200 FRET/mCerulean3 ratios are equivalent to 21 % w/w and 30 % w/w Ficoll, respectively.(19)

201 The FRET/mCerulean3 ratio follows the OD_{600} by returning to the pre-upshift level within 1 h.

202 After this, the FRET/mCerulean3 decreases further to 1.00 ± 0.006 (s.e.m.; n = 90) over an

203 additional 1-2 h, where it remains for at least 23 h. This FRET/mCerulean3 ratio is equivalent

204 to 13 % w/w Ficoll.(19) We maintain the cells in the exponential phase of growth by

205 continuously refreshing the medium. The observations are similar for the crG18 sensor that

206 contains a different linker (Fig. S1).(22) We find that addition of 100 mM NaCl does not lead

207 to significant changes, while the addition of 500 mM NaCl provides a decrease similar to 300

208 mM NaCl (Fig. S2). This apparent threshold coincides with the occurrence of membrane

209 invaginations when 300 and 500 mM NaCl is added, which does not occur with 100 mM

210 NaCl (see also (25) and (2)).

8

211   To confirm that the ratiometric FRET reports genuine changes in excluded volume, rather

212   than e.g. binding of specific molecules to the sensors, we performed a series of control

213   experiments. We investigated the influence of cell lysate on purified sensor (Fig. S3). We

214   lysed *E. coli* with or without 300 mM NaCl and did not find an effect of the cell-free lysate of 7

215   mg of total protein/ml on purified crG18. Hence, cytoplasmic macromolecules do not

216   specifically interact with the sensors. The same applies for small molecule (metabolites,

217   osmolytes) that are abundant in *E. coli* (19, 22, 26). To confirm that the probes are not

218   truncated in osmotically stressed cells, we performed SDS-PAGE analysis. The gels show

219   intact probes in control and osmotically stressed cells (Fig. S4). To assess whether the

220   mCitrine fluorescence is not quenched by acidification of the cells during adaptation, we

221   excited the mCitrine directly at 488 nm, and we did not find a decrease in intensity (Fig. S5).

222   To show that the ratiometric FRET signal is independent of the maturation of the fluorescent

223   proteins,(24) we exchanged the mCerulean3 with the faster maturing mTurquoise2 (crTC2)

224   and obtained a qualitatively similar readout (Fig. S6). Also exchanging the acceptor to

225   cpmVenus (crcpGE) did not lead to a different result, excluding effects specific to the

226   fluorescent proteins.

227   Next, we benchmarked the diffusion of the probes against GFP under conditions of osmotic

228   stress and adaptation by fluorescence recovery after photobleaching (FRAP) (Fig. 1E). The

229   median diffusion coefficient decreases from 5.6($\pm$1.6) μm^2/s to 1.6($\pm$1.3), and subsequently

230   increases 4h after addition of NaCl to 4.2 ($\pm$0.3). The changes in diffusion do not reflect the

231   FRET of the sensor precisely, likely because factors such as immobile barriers influence

232   diffusion differently.(27) These diffusion coefficients compare to 14.1($\pm$3.8), 1.7($\pm$1.1) and

233   10.3($\pm$3.1), respectively, for diffusion of GFP.(4) The last data value was obtained at 1.02

234   Osm, while our osmolarity cumulates to 0.88 Osm (the osmolarity of MOPS medium + 300

235   mM NaCl). The difference in diffusion coefficients of crGE and GFP correspond with the

236   differences in sizes, but, importantly, the relative changes in mobility indicate that they probe

237   similar biochemical organization of the cytoplasm.

9

238 **Macromolecular crowding relates to cell length until cells divide**

239 Macromolecular crowding should relate to the volume of a cell when the number of inert

240 biomacromolecules is constant. To investigate whether the decrease in crowding indeed

241 relates to volume changes and cell growth, we determined the cell length and volume during

242 adaptation. To estimate the volume of the cells, we performed PALM measurements using

243 the inner membrane protein LacY fused to YPet. We find that the volume decreases by 30%

244 immediately after adding 300 mM NaCl (Fig. 1F), while three hours after the osmotic upshift

245 the volume has recovered to ~1.8 fL, which is 82% of the value before the upshift. When

246 measuring the length of the cells from brightfield images by confocal microscopy (Fig. 1C),

247 we find that cells immediately become shorter by 20 % upon addition of 300 mM NaCl, and

248 the length returns to the value before the osmotic upshift after 30 minutes. After 60-90

249 minutes, the average cell length starts to increase. Afterwards, when most cells divide

250 (doubling time of 2h), apparently in a synchronized manner, the average cell length

251 decreases. After this, the average length remains short in the adapted cells. The decrease in

252 length is more pronounced than in volume, which implies that the adapted cells have an

253 increased diameter. Yet, the overall trend is similar for both the cell length and volume. We

254 find that the crowding relates reciprocally with cell length and cell volume (Fig. 1D). After ~2

255 h, which coincides with the moment the cells divide, the relation between crowding and cell

256 volume no longer holds. We find these trends for both the crGE and the crG18 (Fig. S1).

257 Hence, the results indicate that the crowding as anticipated is proportional to the cell volume

258 after the osmotic upshift, but the relationship changes when cells adapt to the osmotic stress.

259 **Elongation or division are not needed to change crowding**

260 To assess whether cell elongation or division are strictly correlated with crowding during

261 adaptation to osmotic stress, we studied individual cells in microfluidics devices. This allows

262 comparison of cells that adapt to those that do not, and we can dissect whether or not cell

263 division influences the levels of crowding. *E. coli* cells growing in 0.1× MOPS-glucose

264 medium (supplemented with 160 mM NaCl) in microfluidic devices can be analyzed for at

265   least 6 h (Fig. S7). We observed less fluctuation in apparent crowding when cells grew in

266   0.1× MOPS-glucose compared to undiluted MOPS-glucose medium, for which we currently

267   do not have an explanation. Exogenous morpholinopropanesulfonate (MOPS) accumulates

268   in *E. coli*(29) and may disturb its physiology. We found that the growth rate in 0.1× MOPS-

269   glucose and MOPS-glucose medium are similar in a liquid culture, which is ~0.5 h^{-1}. Hence,

270   for all the experiments in the microfluidic chamber, we incubated the cells in 0.1× MOPS-

271   glucose, supplemented with 160 mM NaCl to obtain the same osmolarity as MOPS-glucose

272   medium.

273   We incubated the cells in the microfluidic chamber for 2 h, after which we replaced the

274   medium with 0.1× MOPS-glucose with 460 mM NaCl (hence 300 mM extra). To confirm that

275   crowding changes are independent of the type of crowding sensor, we compared the FRET

276   signals of crGE, crE6G2 and crG18 during the osmotic upshift. We find a similar decrease in

277   ratiometric FRET as observed in the experiments in batch culture. We further applied an

278   osmotic upshift with sorbitol, showing a similar response as equiosmolar amounts of sodium

279   chloride (Fig. S8). We counted the number of cells and noted that the cell number increased

280   steadily until the osmotic upshift, after which the osmotic stress reduces the increase

281   temporally (Fig. S9).

282   We previously found that of the three probes crE6G2 was most sensitive to changes in

283   macromolecular crowding.(22) Single cell analyses provides a significant amount of noise

284   (Fig. 2AC), yet for most cells the trend in the FRET/mCerulean3 ratio could clearly be

285   distinguished with crE6G2, allowing comparison of crowding with cell length and division time

286   (Fig. 2B). The single cells showed a transient decrease in length in the first 5 minutes after

287   osmotic upshift, which coincides with the presence of membrane invaginations. After 5 to 10

288   minutes, the cells started to elongate again. Upon addition of 300 mM NaCl, the shape of the

289   FRET/mCerulean3 response of individual cells is similar to that of ensemble measurements.

290   Although the single cell FRET/mCerulean3 data are noisy, we infer that cell division is not

291   strictly correlated with the macromolecular crowding: Cell division appears to be rather

11

292   stochastic and unrelated to the FRET/mCerulean3 curve, which is similar for most of the

293   cells. Furthermore, when we compiled data of cells that grew and compared those that did

294   not grow, we do not observe a significant difference in crowding levels (Fig. 2D). In both

295   cases we find the decrease to be significant (p<0.05, student´s t test). Hence, elongation and

296   division do not necessarily drive the decrease in crowding upon adaptation to 300 mM NaCl,

297   but they coincide with the crowding changes on the population level.

298   **Energy decoupling also decreases crowding**

299   Next, we determined the crowding in cells that were deprived of energy by using a

300   protonophore (FCCP) to dissipate the electrochemical proton gradient, and thereby deplete

301   the cells of ATP. Energy-depleted *E. coli* cells undergo a transition in their internal

302   organization that hampers diffusion of 100 nm-sized but not 10 nm-sized particles.(1) Our

303   probes are in the 10 nm size range, that is, our probes behave as a disordered protein with a

304   distance between the centers of the fluorescent proteins of ~5-10 nm. Therefore, if crowding

305   would be the only factor influencing diffusion, 10 nm particles should not experience a

306   change in crowding because their diffusion does not change. If, on the other hand, native

307   biomacromolecules are assembled into larger structures, e.g. resulting in a transition of the

308   cytoplasm from a fluid into a more solid-like "colloidal glassy" state (1, 30), an inert 10 nm

309   particle could experience less crowding. Such a state could be enhanced by the depletion of

310   ATP, because ATP has been implicated as biological hydrotrope to enhance the solubility of

311   proteins (31).

312   Because the effectiveness of protonophores depends on various factors (e.g. membrane

313   concentration, *E. coli* strain, carbon source, medium pH), we first assessed the FCCP

314   concentration required to halt cell growth and found that 100 μM was necessary under our

315   experimental conditions (Fig. 3A). Next, we applied FCCP to exponentially growing *E. coli*

316   cells that contained the crGE probe, and measured the FRET/mCerulean3 ratios (Fig. 3B).

317   The measurements were performed within two minutes after addition of FCCP. We find that

318   the FRET/mCerulean3 ratio drops upon addition of FCCP and reaches values comparable to

319   those of cells adapted to 300 mM NaCl. We thus conclude that the effective excluded volume

320   probed by crGE of 300 mM NaCl-adapted and energy-depleted cells are similar.

DISCUSSION

322   We have used previously developed crowding sensors to probe changes in excluded volume

323   of *E. coli* cells upon osmotic stress and energy depletion. We show that the effective

324   excluded volume of *E. coli* increases upon osmotic upshift, but subsequently decreases to

325   values below those of unstressed cells. We find that in the first 1-2h the changes in crowding

326   relate in a reciprocal manner to the cytoplasmic volume. When cells adapt to osmotic upshift

327   conditions (300 mM NaCl), the apparent crowding levels become lower than those of

328   unstressed cells.

329   Simply based on the biopolymer volume fraction, one would expect an increased

330   macromolecular crowding in cells that have adapted to growth at increased osmolarities. Yet,

331   Konopka et al. already showed for the first time that the diffusion of GFP was too high

332   compared to what was expected from the biopolymer volume fraction.(4) This in combination

333   with our result confirms that the biopolymer volume fraction is not the sole determinant of

334   crowding effects, which can be expected from theory(8) and suggests that there is a

335   structural change in the cytoplasm. Indeed, the group of Hwa recently showed that cells

336   adapted to hyperosmotic stress have a higher ribosome to overall protein ratio than before

337   osmotic stress.(18) This could explain the altered dependence on the volume fraction:

338   Ribosomes are about 20 nm in diameter while our probes contain a disordered domain and

339   are in the range of 5-10 nm, and thus should exert less of a classical excluded volume effect

340   compared to a smaller protein crowder. Moreover, if the ribosome is attached to mRNA, its

341   effective size is much larger and it would not diffuse freely, which is needed for classical

342   crowding effects. The group of Holt recently investigated the size-dependence of crowding

343   induced by ribosomes in yeast cells (32) and showed that an increased ribosome

344   concentration reduced the lateral diffusion of particles in a size-dependent manner: 40 nm

345   particles had a lower diffusion coefficient than 20 nm particles, while diffusion of 5 nm sized

13

346   particles was not influenced. Thus, an increase in ribosome to overall protein ratio at the

347   same biopolymer volume fraction would diminish the crowding effect.

348   The reciprocal relation between the cell volume and crowding during the first 1-2 hours after

349   the osmotic upshift shows that the macromolecular crowding behaves in a manner that one

350   would expect from concentrating and diluting a solution of inert crowders. After this, or

351   concomitantly, a major change in the biochemical transition may occur and the relation

352   between cell volume and apparent crowding no longer holds. We cannot make a precise

353   comparison of these time scales with literature data given that the media, strain, and

354   magnitude of the upshift varies between experiments. But compatible solutes have a

355   significant influence, a role that the MOPS in our medium could assume.(29) The initial

356   response of cell elongation or volume growth after osmotic upshifts has been reported to

357   occur within a few minutes,(33-35) similar to what we observed in microfluidics for cell length.

358   The time course of the crowding transition of 1-2 hours is in the range of biopolymer

359   synthesis (and changing the proteome) and proceeds throughout the cell division stage.

360   Therefore, even though cell elongation resumes rapidly after shock, a new proteome needs

361   to be synthesized to arrive at a new crowding homeostasis over longer periods. The change

362   in crowding may be assisted by the biosynthesis of e.g. trehalose, which has been reported

363   to accumulate to maximum values in up to an hour in *E. coli* grown in medium without

364   compatible solutes.(36) Although the DNA content can increase under hyperosmotic

365   stress,(37) especially under higher osmotic shocks than we use, we do not consider the DNA

366   a classical crowder due to its large size and immobility. However, DNA could have an indirect

367   effect by reducing the total available volume for other crowders or act through confinement

368   mechanisms. Together, the kinetics of cell length and crowding suggest that the crowding

369   changes are initially governed by cell volume, after which the cytoplasm arrives at a new

370   state through biopolymer synthesis.

371   Although we consider an increase in the ribosome fraction of the total biopolymer content a

372   likely source of the decrease in effective macromolecular crowding, other phenomena could

14

373   contribute. For example, we show here that energy dissipation decreases the effective

374   excluded volume as well, which is an effect that occurs within 2 minutes, which is too fast for

375   major changes in the proteome or/and ribosome content. Here, we achieve perhaps a state

376   where the cytoplasm is more gel-like or colloidal glassy and thus leaves more uncrowded

377   spaces for the probes to occupy.(38) Moreover, even if the sensor and the cytoplasm were

378   homogeneously mixed, crowder self-associations would decrease the excluded volume

379   effect of the crowders.(11) Such a state could be enhanced by the absence of ATP that

380   potentially acts as a hydrotope and solubilizes the proteome.(31) Hence, different

381   biochemical states of the cytoplasm could yield the same effective excluded volume.

382   **CONCLUSION**

383   Cells adapt to external stress to maintain cell growth. We mapped the changes in

384   macromolecular crowding during adaptation to an osmotic upshift, a condition previously

385   shown to alter the biochemical organization of the cell. We show that the cells indeed arrive

386   at a new state where the effect of the excluded volume is decreased, which may be caused

387   by alteration in the particle size distribution in the cytoplasm or change in biochemical

388   organization. This would provide a mechanism to adopt higher biopolymer volume fractions

389   while maintaining an effective crowding homeostasis with excluded volume effects tuned by

390   the particle size and/or mobility.

391   **ACKNOWLEDGEMENTS**

396   **REFERENCES**

397   1.   Parry BR, Surovtsev IV, Cabeen MT, O'Hern CS, Dufresne ER, Jacobs-Wagner C. 2014. The
398   bacterial cytoplasm has glass-like properties and is fluidized by metabolic activity. Cell
399   156:183-94.

15

400   2.   Konopka MC, Shkel IA, Cayley S, Record MT, Weisshaar JC. 2006. Crowding and confinement
401   effects on protein diffusion in vivo. J Bacteriol 188:6115-23.
402   3.   Mika JT, van den Bogaart G, Veenhoff L, Krasnikov V, Poolman B. 2010. Molecular sieving
403   properties of the cytoplasm of Escherichia coli and consequences of osmotic stress. Mol
404   Microbiol 77:200-7.
405   4.   Konopka MC, Sochacki KA, Bratton BP, Shkel IA, Record MT, Weisshaar JC. 2009. Cytoplasmic
406   protein mobility in osmotically stressed Escherichia coli. J Bacteriol 191:231-7.
407   5.   van den Bogaart G, Hermans N, Krasnikov V, Poolman B. 2007. Protein mobility and diffusive
408   barriers in Escherichia coli: consequences of osmotic stress. Mol Microbiol 64:858-71.
409   6.   Mika JT, Poolman B. 2011. Macromolecule diffusion and confinement in prokaryotic cells.
410   Curr Opin Biotechnol 22:117-26.
411   7.   Zhou HX, Rivas G, Minton AP. 2008. Macromolecular crowding and confinement:
412   biochemical, biophysical, and potential physiological consequences. Annu Rev Biophys
413   37:375-97.
414   8.   Rivas G, Minton AP. 2016. Macromolecular Crowding In Vitro, In Vivo, and In Between.
415   Trends Biochem Sci 41:970-981.
416   9.   van den Berg J, Boersma AJ, Poolman B. 2017. Microorganisms maintain crowding
417   homeostasis. Nat Rev Microbiol 15:309-318.
418   10. Rivas G, Minton AP. 2018. Toward an understanding of biochemical equilibria within living
419   cells. Biophys Rev 10:241-253.
420   11. Hall D, Minton AP. 2003. Macromolecular crowding: qualitative and semiquantitative
421   successes, quantitative challenges. Biochim Biophys Acta 1649:127-39.
422   12. Record MT, Jr., Courtenay ES, Cayley DS, Guttman HJ. 1998. Responses of E. coli to osmotic
423   stress: large changes in amounts of cytoplasmic solutes and water. Trends Biochem Sci
424   23:143-8.
425   13. Wood JM. 2015. Bacterial responses to osmotic challenges. J Gen Physiol 145:381-8.
426   14. Shabala L, Bowman J, Brown J, Ross T, McMeekin T, Shabala S. 2009. Ion transport and
427   osmotic adjustment in Escherichia coli in response to ionic and non-ionic osmotica. Environ
428   Microbiol 11:137-48.
429   15. Cheung KJ, Badarinarayana V, Selinger DW, Janse D, Church GM. 2003. A microarray-based
430   antibiotic screen identifies a regulatory role for supercoiling in the osmotic stress response of
431   Escherichia coli. Genome Res 13:206-15.
432   16. Zhao P, Zhou Z, Zhang W, Lin M, Chen M, Wei G. 2015. Global transcriptional analysis of
433   Escherichia coli expressing IrrE, a regulator from Deinococcus radiodurans, in response to
434   NaCl shock. Mol Biosyst 11:1165-71.
435   17. Metris A, George SM, Mulholland F, Carter AT, Baranyi J. 2014. Metabolic shift of Escherichia
436   coli under salt stress in the presence of glycine betaine. Appl Environ Microbiol 80:4745-56.
437   18. Dai X, Zhu M, Warren M, Balakrishnan R, Okano H, Williamson JR, Fredrick K, Hwa T. 2018.
438   Slowdown of Translational Elongation in Escherichia coli under Hyperosmotic Stress. MBio 9.
439   19. Boersma AJ, Zuhorn IS, Poolman B. 2015. A sensor for quantification of macromolecular
440   crowding in living cells. Nat Methods 12:227-9, 1 p following 229.
441   20. Sukenik S, Ren P, Gruebele M. 2017. Weak protein-protein interactions in live cells are
442   quantified by cell-volume modulation. Proc Natl Acad Sci U S A 114:6776-6781.
443   21. Gnutt D, Brylski O, Edengeiser E, Havenith M, Ebbinghaus S. 2017. Imperfect crowding
444   adaptation of mammalian cells towards osmotic stress and its modulation by osmolytes. Mol
445   Biosyst 13:2218-2221.
446   22. Liu B, Aberg C, van Eerden FJ, Marrink SJ, Poolman B, Boersma AJ. 2017. Design and
447   Properties of Genetically Encoded Probes for Sensing Macromolecular Crowding. Biophys J
448   112:1929-1939.
449   23. van den Berg J, Galbiati H, Rasmussen A, Miller S, Poolman B. 2016. On the mobility,
450   membrane location and functionality of mechanosensitive channels in Escherichia coli. Sci
451   Rep 6:32709.

452   24.   Liu B, Mavrova SN, van den Berg J, Kristensen SK, Mantovanelli L, Veenhoff LM, Poolman B,
453   Boersma AJ. 2018. Influence of Fluorescent Protein Maturation on FRET Measurements in
454   Living Cells. ACS Sens 3:1735-1742.
455   25.   Mika JT, Schavemaker PE, Krasnikov V, Poolman B. 2014. Impact of osmotic stress on protein
456   diffusion in Lactococcus lactis. Mol Microbiol 94:857-70.
457   26.   Liu BQ, Poolman B, Boersma AJ. 2017. Ionic Strength Sensing in Living Cells. Acs Chemical
458   Biology 12:2510-2514.
459   27.   Schavemaker PE, Boersma AJ, Poolman B. 2018. How Important Is Protein Diffusion in
460   Prokaryotes? Front Mol Biosci 5:93.
461   28.   Schavemaker PE, Smigiel WM, Poolman B. 2017. Ribosome surface properties may impose
462   limits on the nature of the cytoplasmic proteome. Elife 6.
463   29.   Cayley S, Record MT, Jr., Lewis BA. 1989. Accumulation of 3-(N-morpholino)propanesulfonate
464   by osmotically stressed Escherichia coli K-12. J Bacteriol 171:3597-602.
465   30.   Mittasch M, Gross P, Nestler M, Fritsch AW, Iserman C, Kar M, Munder M, Voigt A, Alberti S,
466   Grill SW, Kreysing M. 2018. Non-invasive perturbations of intracellular flow reveal physical
467   principles of cell organization. Nat Cell Biol 20:344-351.
468   31.   Patel A, Malinovska L, Saha S, Wang J, Alberti S, Krishnan Y, Hyman AA. 2017. ATP as a
469   biological hydrotrope. Science 356:753-756.
470   32.   Delarue M, Brittingham GP, Pfeffer S, Surovtsev IV, Pinglay S, Kennedy KJ, Schaffer M,
471   Gutierrez JI, Sang D, Poterewicz G, Chung JK, Plitzko JM, Groves JT, Jacobs-Wagner C, Engel
472   BD, Holt LJ. 2018. mTORC1 Controls Phase Separation and the Biophysical Properties of the
473   Cytoplasm by Tuning Crowding. Cell 174:338-349 e20.
474   33.   Rojas E, Theriot JA, Huang KC. 2014. Response of Escherichia coli growth rate to osmotic
475   shock. Proc Natl Acad Sci U S A 111:7807-12.
476   34.   Pilizota T, Shaevitz JW. 2012. Fast, multiphase volume adaptation to hyperosmotic shock by
477   Escherichia coli. PLoS One 7:e35205.
478   35.   Pilizota T, Shaevitz JW. 2014. Origins of Escherichia coli growth rate and cell shape changes at
479   high external osmolality. Biophys J 107:1962-1969.
480   36.   Dinnbier U, Limpinsel E, Schmid R, Bakker EP. 1988. Transient accumulation of potassium
481   glutamate and its replacement by trehalose during adaptation of growing cells of Escherichia
482   coli K-12 to elevated sodium chloride concentrations. Arch Microbiol 150:348-57.
483   37.   Dai X, Zhu M. 2018. High Osmolarity Modulates Bacterial Cell Size through Reducing Initiation
484   Volume in Escherichia coli. mSphere 3.
485   38.   Spitzer J, Poolman B. 2013. How crowded is the prokaryotic cytoplasm? FEBS Lett 587:2094-
486   8.

487

488

489

490
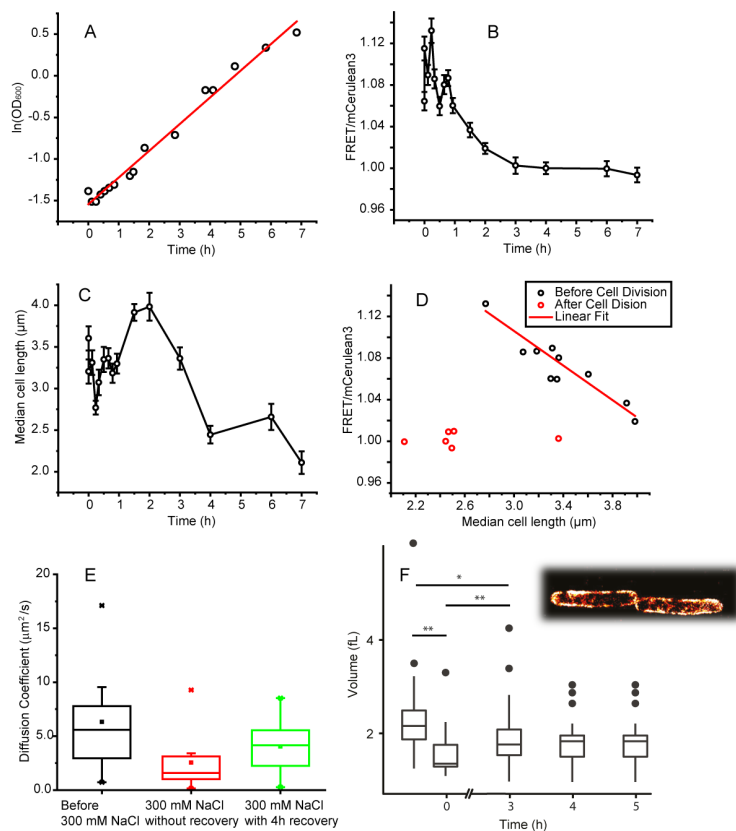
Figure 1. Response of *E. coli* BL21(DE3) containing the crGE probe in pRSET A to the

addition of 300 mM NaCl. **A**. The ln(OD_{600}) decreases after the upshift and subsequently

increases linearly over time (passing the pre-upshift OD_{600} after ~1h). The OD_{600} is corrected

for continuous dilution of the culture to maintain the OD_{600} between 0.1 and 0.3. The data fits

a linear curve with R^2=0.99, indicating exponential growth throughout the course of the

experiment. **B**. The FRET/mCerulean3 ratio of the crGE probe as measured by confocal

fluorescence microscopy. The ratios immediately increase after osmotic upshift and decrease

after one hour to levels lower than prior to the osmotic upshift. All data is for at least 60 *E.*

coli cells, with a FRET/mCerulean3 standard deviation of ~0.05 and a standard error of

~0.009. **C**. Osmotic upshift results in a decrease in median cell length as measured by

fluorescence microscopy (same cells as in panel B), which is followed by an increase in

length of the synchronized cells until division starts, resulting in smaller cells compared to

pre-upshift conditions. **D**. Data from panel B and C combined showing the relation (linear

504 approximation: R^2=0.82) between the FRET/mCerulean3 ratio and the median cell length

505 (black circles), which holds until the cells divide. After that, the FRET/mCerulean3 remains

506 low (red circles), which is after t=3h in panel B and C. **E**. Lateral diffusion of the crGE probe

507 in unstressed, and 300 mM NaCl stressed and adapted cells. The FRAP measurements

508 were carried out as described previously.(28) Displayed are the box plots generated for

509 measurements of 10-20 cells, each from the same culture to allow comparison. Box

510 represents 25-75% of the data range, whiskers is within the 1.5 interquartile range, bar in the

511 box is median, square is average, and stars are outliers. **F**. Cell volume changes during

512 hyperosmotic stress. *E. coli* BL21(DE3) expressing LacY-YPet was used and the contours

513 from single-molecule localizations by PALM were used to obtain the volumes of the cells

514 (see caption). Untreated cells are measured at t = -1h in MOPS-glucose; to capture the data

515 point at t = 0h, the cells were resuspended in MOPS medium without potassium and glucose

516 to prevent recovery, and subsequently treated with 300 mM NaCl. For time points 3, 4 and

517 5h cells were left to adapt to 300 mM NaCl in regular MOPS-glucose medium. For each data

518 point, ~30 cells were imaged and analyzed (*P<0.05, **P<0.005, paired sample t-test).

519

520

521

522
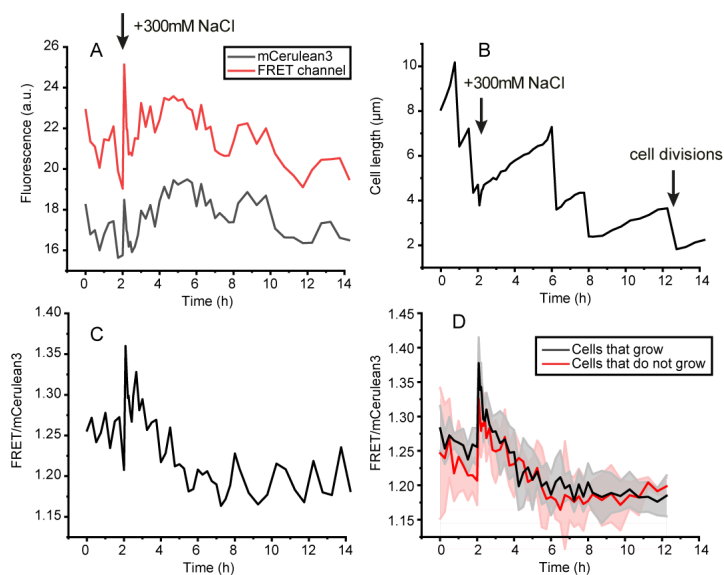
Figure 2. Single cell analysis in microfluidics, monitored by confocal microscopy. At 2h, the medium flown into the chamber that holds the cells was changed from 0.1×MOPS +160 mM NaCl to 0.1×MOPS +460 mM NaCl (net increase 300 mM NaCl). The *E. coli* BL21(DE3) cells contained the crE6G2 sensor in pRSET A. **A**. Fluorescence intensity of a single cell over time; the emission from the mCerulean3 and the FRET channel are shown. **B**. Cell length of the same cell analyzed in panel A, showing elongation and cell division and a small transient decrease in cell length following the osmotic upshift at t=2h. The time between cell divisions varies significantly. **C**. The FRET/mCerulean3 ratio of the same cell, showing a qualitatively similar time course of the crowding as in the batch experiments. **D**. Average of the population of cells that grow after osmotic upshift (n=9) compared with cells that do not grow (n=4). Shaded areas are the corresponding standard deviations.

535
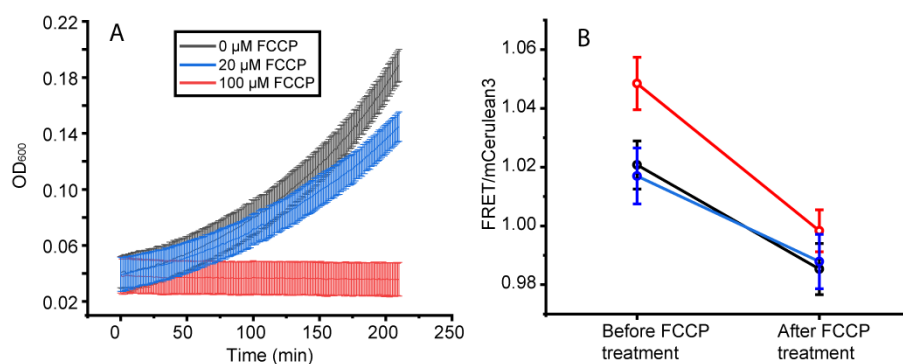
Figure 3. Crowding of energy-depleted *E. coli* as probed by crGE. **A**. The effect of FCCP on

the growth of *E. coli* BL21(DE3) in MOPS minimal medium supplemented with glucose. Error

bars are four technical repeats. **B**. Application of 100 μM of FCCP results in an immediate

drop in the FRET/mCerulean3 ratio. Three independent biological repeats are displayed;

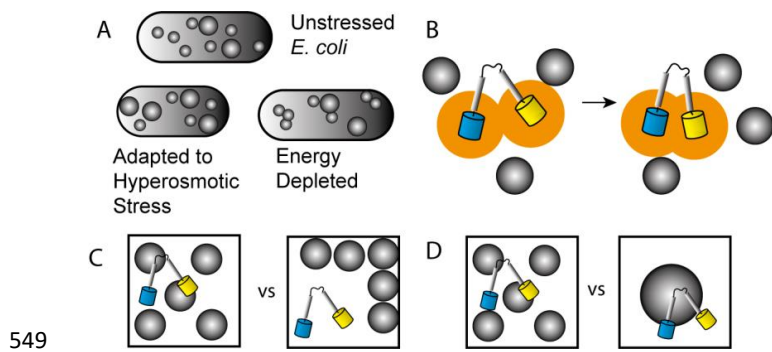error bars are error in the fit of FRET versus mCerulean3 intensity over about 100 cells.

549

550 **Figure 4**. Changes in biochemical organization that affect crowding in cells. **A**. Adaptation to

551 osmotic stress and energy depletion changes both the size and spatial distribution of the

552 macromolecules. **B**. Working mechanism behind probe compression: The excluded volume

553 excluded (orange) reduces due to crowding. This is caused by i) increasing the translational

554 degrees of freedom for the crowders; and ii) an osmotic pressure difference (depletion force)

555 between the bulk and the crowder-inaccessible volume within the probe. **C**. Immobile

556 crowders do not affect the behavior described in Fig 4B. Additionally, spatial heterogeneity

557 increases the distance between probe and crowder and reduces frequency of collision. **D**. At

558 similar volume fraction, smaller crowders provide more entropy gain by virtue of number

559 density and larger osmotic pressure differences.

560

22